Journal of Science and Transport Technology
Journal homepage: https://jstt.vn/index.php/en

Effect of various factors on heat transfer characteristics of steady magnetohydrodynamic casson nanofluid (Cu+Water) between two infinite parallel plates by Akbari Ganji's method considering Cattaneo–Christov heat flux model

A. El Harfouf[1], Dung Nguyen Trong[2,3], H. Mes-adi[4], Sanaa Hayani Mounir[1], Umut Saraç[5], Quoc Tuan Tran[6,*], Van Cao Long[2], Ştefan Ţălu[7]

[1]Sultan Moulay Slimane University of Beni Mellal, 25000, Khouribga, Morocco
[2]University of Zielona Góra, 65-516 Zielona Góra, Poland
[3]Hanoi National University of Education, Hanoi, 100000, Vietnam
[4]Université Sultan Moulay Slimane - Beni Mellal, 25000, Khouribga, Maroc
[5]Bartın University, 74100, Bartın, Turkey
[6]Faculty of Basic Science, University of Transport Technology, 54 Trieu Khuc, Thanh Xuan, Hanoi 100000, Vietnam
[7]Technical University of Cluj-Napoca, 400020, Cluj County, Romania

Article info
Type of article:
Original research paper

DOI:
https://doi.org/10.58845/jstt.utt.2023.en.3.1.53-67

***Corresponding author:**
E-mail address:
tuantq@utt.edu.vn

Received: 08/03/2023
Revised: 23/03/2023
Accepted: 24/03/2023

Abstract: In this study, the influence of various factors on the heat transfer characteristics of the steady magnetohydrodynamic Casson nanofluid (Cu+Water) between two infinite parallel plates considering the Cattaneo–Christov heat flux model is explored by means of the Akbari Ganji's Method. The values of Nusselt number N_u^* are also determined for different values of viscosity, magnetic, and volume fraction parameters and various metallic and nonmetallic nanoparticles (NPs). The findings reveal that the temperature profile (TP) decreases with rising casson fluid and thermal relaxation parameters. However, an increment in the TP is detected for large values of the volume fraction parameter, radiation parameter, Prandtl number, and Eckert number. It is found that the N_u^* varies proportionally with the viscosity and volume fraction parameters, but it is inversely proportional to the magnetic parameter. The results also show that different metallic and nonmetallic NPs have different values of N_u^*.

Keywords: Magnetohydrodynamic Casson Nanofluid, Akbari Ganji's Method, Magnetic field, Cattaneo-Christov Heat Flux Model, Heat Transfer Characteristics.

1. Introduction

In recent years, researchers have focused on non-Newtonian fluids, which have important engineering and industrial applications [1-4]. However, it is very difficult to analyze non-Newtonian fluids because of their complexity [5].

Therefore, researchers suggested different models to examine them such as Casson, micropolar, viscoelastic, etc [5,6]. The Casson fuid is classifed as a non-Newtonian fuid because of its rheological properties [3]. The Casson fluid is a shear thinning liquid with infinite viscosity at zero shear rates and zero viscosity at infinite shear rates [3,5,7]. The study examined the influence of chemical reaction on Casson fluid flow over an inclined porous plate [8]. Another study investigated the momentum and heat transfer properties of Casson fluid flow over an inclined plate [9].

The nanofluids consist of the base fluid (oil and water) containing carbide, metal, and oxide nanoparticles (NPs) [3,10,11]. They are special functional fluids that are very useful for raising the heat transfer rate, increasing the thermal conductivity, and reducing the energy loss [10, 11]. In addition, there are some studies on the Magnetohydrodynamic (MHD) Casson nonofluids. A numerical study showed that the presence of magnetic fields enhances the thermal transfer [12]. In another numerical study by Chamkha et al. [13], it was shown that the Nusselt number N_u^* is more significantly affected by laminar NPs than other NPs. The role of diverse parameters on the temperature and concentration profiles of steady MHD nanofluid between parallel plates was also established [14].

Many different numerical and analytical methods such as Differential Transformation Method (DTM) [14-17], Homotopy Perturbation Method (HPM) [18-22], Akbari Ganji's Method (AGM) [7,23], Runge-Kutta Method (RKM) [5,11, 24,25], etc. have been applied to various problems in the fields of science and engineering. Among them, the AGM is one of the more recent and effective semi-analytical methods [7]. Furthermore, it is efficient and has sufficient accuracy compared to other semi-analytical and numerical methods [7,23].

To explore the thermal relaxation time characteristic, the Cattaneo-Christov Heat Flux (CCHF) model is assumed thermally. The study revealed the analytical solutions for the temperature governing equation via CCHF model for coupled flow and heat transfer of an upper-convected Maxwell fluid [26]. The study explored the spinning flow of viscoelastic fluids due to a stretching sheet by means of the CCHF model [27]. In another research, the steady three-dimensional boundary layer flow and heat transfer characteristics to Burgers fluid was studied by employing the CCHF model [28]. Considering the CCHF model, the efficiency of the binary chemical reaction on MHD Casson fluid was explored by Reddy et al [29]. The study also examined the unsteady squeezing MHD nanofluid flow and heat transfer between two parallel plates considering the CCHF model [30]. The results indicated that the N_u^* increased (decreased) with increasing heat source (thermal relaxation) parameter. It was also reported that the temperature profile (TP) decreased with enhancing volume fraction, magnetic, and thermal relaxation parameters and increased with increasing radiation parameter and squeeze number [30]. Other related studies on the simulation of nanofluids and heat transfer are also available in the literature [31–33]. The influence of various factors on the structural and mechanical features of a wide variety of metallic NPs such as Ni [34,35], Fe [36], AlNi [37], NiFe [38], etc., has been examined in recent studies using the molecular dynamic simulation method. In addition, in a very recent study [7], the analytic solution of steady two-dimensional laminar MHD flow of incompressible viscous nanofluids between two parallel plates has also been discussed by means of the AGM. The results showed that an increase in the magnetic and viscosity parameters induced a decrease in the velocity profile. It was also revealed that the skin friction coefficient increased with rising viscosity, magnetic, and volume fraction parameters [7]. This study aims to explore the impact of various

factors on the heat transfer characteristics of steady MHD Casson nanofluid (Cu+Water) between two infinite parallel plates considering the CCHF model by means of the AGM. The values of N_u^* are also calculated for various factors and metallic and nonmetallic NPs.

2. Calculation method

2.1. Description of the problem

We consider a steady MHD Casson nanofluid (Cu+Water) flow between two infinite parallel plates. As depicted in Fig 1, two infinite parallel plates are placed horizontally at $y = 0$ and $y = h$. The x-direction extends along the plate while the y-direction is vertical to the plate. To examine the various factors on the heat transfer characteristics, the CCHF model is applied instead of the classical Fourier's theory. The nanofluid is incompressible and considered non-Newtonian. A uniform magnetic field B_0 is also considered.

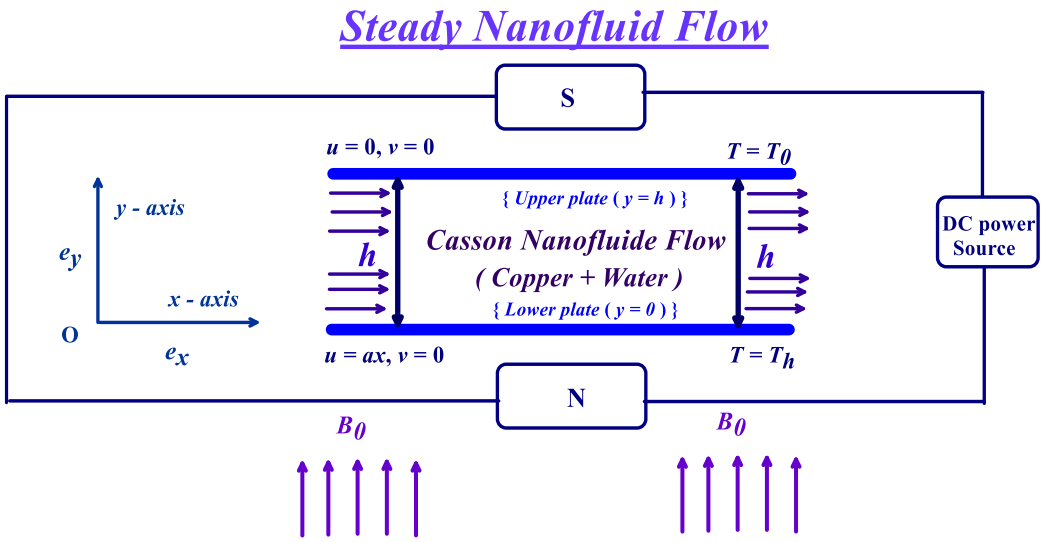

Fig 1. Schematic model of the present work

2.2. The equations of model

2.2.1. The continuity equation

The nanofluid is considered incompressible, and thus the continuity equation is defined:

$$\frac{\partial u}{\partial x}+\frac{\partial v}{\partial y}=0$$

(Equation 1)

2.2.2. The momentum equation

Under the conditions mentioned above, the contribution of the electric force is negligible compared to the contribution of the magnetic force, thus the governing equations for momentum are as follows:

$$\rho_{nf}\left(\mathbf{V}.\nabla\right)\mathbf{V}=\rho_{nf}\mathbf{g}+\nabla.\bar{\sigma}+\mathbf{J}\times\mathbf{B}$$

(Equation 2)

Where $\rho_{nf}\mathbf{g}$ is the buoyancy force, $\mathbf{J}\times\mathbf{B}$ is magnetic force with $\mathbf{J}=\sigma_{nf}\left(\mathbf{V}\times\mathbf{B}\right)$, σ_{nf} represents the electrical conductivity, $\mathbf{V}=(u,v)$ is velocity vector, $\mathbf{B}=(0,B_0)$ is the magnetic field, $\bar{\sigma}=\begin{bmatrix}\sigma_{xx} & \tau_{xy}\\ \tau_{yx} & \sigma_{yy}\end{bmatrix}=-p\mathbf{I}+\bar{\tau}$ is the Cauchy stress tensor. Hence, we get that: $\mathbf{J}\times\mathbf{B}=-u_{nf}B_0^2\mathbf{e_x}$.

Where $\sigma, \tau, \mathbf{I}$ and $\bar{\tau}$ correspond to the normal stress, shear stress, 2×2 identity matrix, and deviatoric stress tensor, respectively.

It should be noted here that the mechanical pressure (p) is $p=-\frac{1}{3}\left(\sigma_{xx}+\sigma_{yy}\right)$.

Finally we get:

$$\rho_{nf}\left(V.\nabla\right)V=-\nabla P+\nabla\cdot\bar{\tau}-\sigma_{nf}B_0^2e_x$$

(Equation 3)

Non-Newtonian Casson nanofluid model:

In equation (3), the term $\nabla.\bar{\tau}$ corresponds to

divergence of the stress tensor and it is described as:

$$\nabla.\bar{\tau} = \left(\frac{\partial \tau_{xx}}{\partial x} + \frac{\partial \tau_{xy}}{\partial y}\right)_{\mathbf{e_x}} + \left(\frac{\partial \tau_{yy}}{\partial y} + \frac{\partial \tau_{xy}}{\partial x}\right)_{\mathbf{e_y}}$$

(Equation 4)

For two directions $(Ox)\,\text{and}\,(Oy)$, the following equations can be obtained:

Projection on the x direction:

$$\left(u\frac{\partial u}{\partial x} + v\frac{\partial u}{\partial y}\right) = -\frac{1}{\rho_{nf}}\frac{\partial p}{\partial x} + \frac{\mu_{nf}}{\rho_{nf}}\left(1+\frac{1}{\beta}\right)\left(2\frac{\partial^2 u}{\partial x^2} + \frac{\partial^2 u}{\partial y^2} + \frac{\partial^2 v}{\partial y \partial x}\right) - B_0^2\frac{\sigma_{nf}}{\rho_{nf}}u$$

(Equation 5)

Where $\beta = \frac{\mu_B\sqrt{2\pi_c}}{p_y}$ is the Casson fluid parameter.

Projection on the y direction:

$$\left(u\frac{\partial v}{\partial x} + v\frac{\partial v}{\partial y}\right) = -\frac{1}{\rho_{nf}}\frac{\partial p}{\partial y} + \frac{\mu_{nf}}{\rho_{nf}}\left(1+\frac{1}{\beta}\right)\left(2\frac{\partial^2 v}{\partial y^2} + \frac{\partial^2 v}{\partial x^2} + \frac{\partial^2 u}{\partial y \partial x}\right)$$

(Equation 6)

If we do $\frac{\partial(6)}{\partial x} - \frac{\partial(5)}{\partial x}$, we get that:

$$u\frac{\partial \omega}{\partial x} + v\frac{\partial \omega}{\partial y} = \frac{\mu_{nf}}{\rho_{nf}}\left(1+\frac{1}{\beta}\right)\left(2\frac{\partial^3 v}{\partial x \partial y^2} + \frac{\partial^3 v}{\partial x^3} - \frac{\partial^3 u}{\partial y^3} + B_0^2\frac{\sigma_{nf}}{\rho_{nf}}\frac{\partial u}{\partial y}\right)$$

(Equation 7)

Where $\omega = \frac{\partial v}{\partial x} - \frac{\partial u}{\partial y}$.

2.2.3. The energy equation

Under the aforementioned conditions, the governing equations for energy are as follows:

$$\left(\rho c_p\right)_{nf}\left(u\frac{\partial T}{\partial x} + v\frac{\partial T}{\partial y}\right) = -(\nabla.\mathbf{q}) - \frac{1}{\left(\rho c_p\right)_{nf}}\frac{\partial q_{rad}}{\partial y} + \frac{\mathbf{J}.\mathbf{J}}{\sigma_{nf}} + \frac{\mu_{nf}}{\left(\rho c_p\right)_{nf}}\left(1+\frac{1}{\beta}\right)\Psi$$

(Equation 8)

Where: $\mathbf{J}.\mathbf{J} = \sigma_{nf}{}^2 B_0^2 u^2$ corresponds to the Joule heating, $\left(\rho c_p\right)_{nf}$ indicates the heat capacity of the nanofluid, μ_{nf} is the dynamic plastic viscosity and $\Psi = \left[2\left(\frac{\partial u}{\partial x}\right)^2 + \left(\frac{\partial u}{\partial y} + \frac{\partial v}{\partial x}\right)^2 + 2\left(\frac{\partial v}{\partial y}\right)^2\right]$ represents the dissipation viscous function in the 2D case form.

q_{rad} represents the radiative heat flux. Applying the Rosseland approximation for radiation we acquire:

$$q_{rad} = -\left(\frac{4\sigma^*}{3k_{nf}^*}\right)\frac{\partial T^4}{\partial y}$$

(Equation 9)

Where σ^* and k_{nf}^* correspond to the Stefan–Boltzmann constant and the mean absorption coefficient, respectively. Moreover, we assume that the temperature difference within the flow is such that T^4 maybe expanded in a Taylor series. Finally, we find:

$$q_{rad} = -\frac{16\sigma^* T_\infty^3}{3k_{nf}^*}\frac{\partial T}{\partial y}$$

(Equation 10)

The heat flux vector q is defined by the following equation according to the CCHF model.

$$\mathbf{q} + \Omega_E\left[\mathbf{V}.(\nabla\mathbf{q}) + (\nabla.\mathbf{V})\mathbf{q} - \mathbf{q}.(\nabla\mathbf{V})\right] = -k_{nf}\nabla T$$

(Equation 11)

Here, Ω_E shows the relaxation time of heat flux and k_{nf} represents the thermal conductivity.

The classical Fourier's law can be derived from equation (11) by applying $\Omega_E = 0$. When the incompressibility of the nanofluid $(\nabla.\mathbf{V} = 0)$ is used in Eq. (11), we have:

$$\mathbf{q} + \Omega_E\left[\mathbf{V}\cdot(\nabla\mathbf{q}) + (\nabla\cdot\mathbf{V})\mathbf{q} - \mathbf{q}\cdot(\nabla\mathbf{V})\right] = -k_{nf}\nabla T$$

(Equation 12)

The flux vector q can be eliminated between the two Eqs. (8) and (12), then we get:

$$\left(\frac{\partial T}{\partial t}+u\frac{\partial T}{\partial x}+v\frac{\partial T}{\partial y}\right)+\Omega_E\Delta_E=$$

$$\frac{k_{nf}}{(\rho c_p)_{nf}}\left(\frac{\partial^2 T}{\partial x^2}+\frac{\partial^2 T}{\partial y^2}\right)-\frac{\partial q_{rad}}{\partial y}+B_0^2\frac{\sigma_{nf}}{(\rho c_p)_{nf}}u^2+$$

$$\frac{\mu_{nf}}{(\rho c_p)_{nf}}\left(1+\frac{1}{\beta}\right)\left[\left[2\left(\frac{\partial u}{\partial x}\right)^2+\left(\frac{\partial u}{\partial y}+\frac{\partial v}{\partial x}\right)^2+2\left(\frac{\partial v}{\partial y}\right)^2\right]\right]$$

(Equation 13)

Where:

$$\Delta_E=u\frac{\partial u}{\partial x}\frac{\partial T}{\partial x}+u^2\frac{\partial^2 T}{\partial x^2}+u\frac{\partial v}{\partial x}\frac{\partial T}{\partial y}+$$

$$v\frac{\partial u}{\partial y}\frac{\partial T}{\partial x}+v\frac{\partial v}{\partial y}\frac{\partial T}{\partial y}+v^2\frac{\partial^2 T}{\partial y^2}+2uv\frac{\partial^2 T}{\partial y\partial x}$$

(Equation 14)

The governing equation for the heat transfer in this problem is given by the following equation:

$$\left(\frac{\partial T}{\partial t}+u\frac{\partial T}{\partial x}+v\frac{\partial T}{\partial y}\right)+\Omega_E\left(u\frac{\partial u}{\partial x}\frac{\partial T}{\partial x}+u^2\frac{\partial^2 T}{\partial x^2}+u\frac{\partial v}{\partial x}\frac{\partial T}{\partial y}\right.$$

$$\left.+v\frac{\partial u}{\partial y}\frac{\partial T}{\partial x}+v\frac{\partial v}{\partial y}\frac{\partial T}{\partial y}+v^2\frac{\partial^2 T}{\partial y^2}+2uv\frac{\partial^2 T}{\partial y\partial x}\right)$$

$$=\frac{k_{nf}}{(\rho c_p)_{nf}}\left(\frac{\partial^2 T}{\partial x^2}+\frac{\partial^2 T}{\partial y^2}\right)-\frac{\partial q_{rad}}{\partial y}+B_0^2\frac{\sigma_{nf}}{(\rho c_p)_{nf}}u^2+$$

$$\frac{\mu_{nf}}{(\rho c_p)_{nf}}\left(1+\frac{1}{\beta}\right)\left[\left[2\left(\frac{\partial u}{\partial x}\right)^2+\left(\frac{\partial u}{\partial y}+\frac{\partial v}{\partial x}\right)^2+2\left(\frac{\partial v}{\partial y}\right)^2\right]\right]$$

(Equation 15)

Here ρ_{nf} corresponds to the effective density, μ_{nf} shows the effective dynamic viscosity, $(\rho c_p)_{nf}$ represents the heat capacity and k_{nf} indicates the thermal conductivity, and σ_{nf} is the electric conductivity of the nanofluid. They are as follows [18]:

$$\rho_{nf}=(1-\Phi)\rho_f+\Phi\rho_p;$$

$$(\rho Cp)_{nf}=(1-\Phi)(\rho Cp)_f+\Phi(\rho Cp)_p$$

(Equation 16)

$$\mu_{nf}=\frac{\mu_f}{(1-\Phi)^{2.5}}$$

(Equation 17)

$$(\rho Cp)_{nf}=(1-\Phi)(\rho Cp)_f+\Phi(\rho Cp)_p$$

(Equation 18)

$$K_{nf}=\frac{K_s+2K_f-2\Phi(K_f-K_s)}{K_s+2K_f+2\Phi(K_f-K_s)}K_f$$

(Equation 19)

$$\sigma_{nf}=\left[1+\frac{3(\sigma_p-\sigma_f)\varphi}{(\sigma_p+2\sigma_f)-(\sigma_p-\sigma_f)\varphi}\right]_f$$

(Equation 20)

2.2.4. The boundary conditions

In this work, the relevant boundary conditions are as follows [14]:

$$u|_{y=0}=ax,\ v|_{y=0}=0,\ T|_{y=0}=T_0,$$

$$u|_{y=h}=0,\ v|_{y=h}=0,\ T|_{y=h}=T_h$$

(Equation 21)

The viscosity parameter R, magnetic parameter M, Prandtl number P_r, radiation parameter N, thermal relaxation parameter β_E, and Eckert number Ec are non-dimensional quantities and they are described as:

$$R=\frac{ah^2}{u_f},\ \delta^2=\frac{h^2}{x^2},\ M=\frac{B_0^2h^2_f}{\rho_f u_f},\ N=\frac{k^*_{nf}k_{nf}}{4\sigma^* T^3_\infty},$$

$$P_r=\frac{\mu_f c_{pf}}{k_f},\ E_c=\frac{\alpha^2x^2}{(T_0-T_h)c_{pf}},\ \beta_E=\alpha\Omega_E$$

(Equation 22)

Here, A_1, A_2, A_3, A_4 and A_5 are dimensionless constants:

$$A_1=\frac{\rho_{nf}}{\rho_f},\ A_2=\frac{\sigma_{nf}}{\sigma_f},\ A_3=\frac{\mu_{nf}}{\mu_f},$$

$$A_4=\frac{k_{nf}}{k_f},\ A_5=\frac{(\rho c_p)_{nf}}{(\rho c_p)_f}$$

(Equation 23)

With these boundary conditions:

$$f'(0)=1,\ f(0)=0,\ \Theta(0)=1\quad \text{at}\quad =0$$

(Equation 24)

$$f'(1)=0,\ f(1)=0,\ \Theta(1)=0\quad \text{at}\quad =1$$

(Equation 25)

The N_u^* in this problem is defined as:

$$N_u^* = \left| A_4 \left(\frac{3N+4}{3N} \right) \theta'(0) \right|$$

(Equation 26)

2.3. Homotopy Perturbation Method (HPM)

2.3.1. Basic Idea of the HPM

In the HPM method, the following equation is considered [39]:

$$A(u) - f(r) = 0, \quad r \in \Omega$$

(Equation 27)

With the boundary condition of:

$$B\left(u, \frac{\partial U}{\partial n}\right) = 0, \quad r \in \Gamma$$

(Equation 28)

Where A and B represent a general differential operator and a boundary operator, respectively. The f (r) corresponds to a known analytical function and Γ indicates the boundary of the domain Ω [39]. A differential operator can be divided into two parts, linear L and nonlinear N. Thus, the Eq. 27 becomes as follows:

$$H(v, p) = (1 - p)\left[L(v) - L(u_0)\right] + p\left[L(v) + N(v) - f(r)\right] = 0$$

(Equation 29)

Where

$$v = v_0 + pv_1 + p^2 v_2 + p^3 v_3 + \ldots$$

(Equation 30)

And:

$$u = \lim_{p \to 1} v = v_0 + v_1 + v_2 + \ldots$$

(Equation 31)

2.3.2. Implementation of the method

According to the HPM, a homotopy can be formed as: (Equation 32)

$$H(\theta, p) = (1-p)\left[\Theta'' - \Theta_0''(0)\right] + p\left[\begin{array}{l} \Theta''(\eta) + \left(\frac{3N}{3N+4}\right)\left(\frac{A_5}{A_4} P_r R\right) f(\eta)\Theta'(\eta) + \\ -\left(\frac{3N}{3N+4}\right)\left(\frac{A_5}{A_4} P_r R \beta_E\right)\left[f(\eta) f'(\eta)\Theta'(\eta) + f^2(\eta)\Theta''(\eta)\right] + \\ +\left(\frac{3N}{3N+4}\right)\left(\frac{A_2}{A_4} P_r M E_c\right) f'^2(\eta) + \\ +\left(\frac{3N}{3N+4}\right)\left(\frac{A_3}{A_4} P_r E_c\right)\left(1 + \frac{1}{\beta}\right)\left[4^2 f'^2(\eta) + f''^2(\eta)\right] \end{array}\right] = 0$$

We consider f and θ as follows:

$$f(\eta) = f_0(\eta) + p^1 f_1(\eta) + p^2 f_2(\eta) + p^3 f_3(\eta) + \ldots = \sum_{i=0}^{N} p^i f_i(\eta)$$

(Equation 33)

$$\theta(\eta) = \theta_0(\eta) + p^1 \theta_1(\eta) + p^2 \theta_2(\eta) + p^3 \theta_3(\eta) + \ldots = \sum_{i=0}^{N} p^i \theta_i(\eta)$$

(Equation 34)

With some rearrangements based on powers of p–terms, we get: $p^0 : f_0'''' = 0,\ \theta_0'' = 0$

Boundary conditions:

$$f_0'(0) = 1,\ f_0(0) = 0,\ \theta_0(0) = 1 \quad \text{at} \quad = 0$$

$$f_0'(1) = 0,\ f_0(1) = 0,\ \theta_0(1) = 0 \quad \text{at} \quad = 1$$

(Equation 35)

The solution of equations is obtained when $p \to 1$, will be as follows:

$$f(\eta) = f_0(\eta) + f_1(\eta) + f_2(\eta) + f_3(\eta) + \ldots = \sum_{i=0}^{N} f_i(\eta)$$

$$\theta(\eta) = \theta_0(\eta) + \theta_1(\eta) + \theta_2(\eta) + \theta_3(\eta) + \ldots = \sum_{i=0}^{N} \theta_i(\eta)$$

(Equation 36)

2.4. Akbari–Ganji's method (AGM)

2.4.1. Basic Idea of the AGM

The general form of equation with the boundary conditions is: (Equation 37)

$$p_k : f\left(u, u', u'', \ldots, u^{(m)}\right) = 0; \quad u = u(x)$$

The nonlinear differential equation of p, the parameter u and their derivatives are considered as follows:

Boundary conditions:

$$\begin{cases} u(x) = u_0, u'(x) = u_1, \ldots, u^{(m-1)}(x) = u_{m-1} & \text{at } x = 0 \\ u(x) = u_{L_0}, u'(x) = u_{L_1}, \ldots, u^{(m-1)}(x) = u_{L_{m-1}} & \text{at } x = L \end{cases}$$

(Equation 38)

We suppose that the solution of this equation is given by:

$$u(x) = \sum_{i=0}^{n} a_i x^i = a_0 + a_1 x^1 + a_2 x^2 + a_3 x^3 \ldots + a_n x^n$$

(Equation 39)

The larger n, the more accurate the solution will be obtained. By inserting Eq. (39) into Eq. (37), the residuals can be obtained. According to

boundary conditions and residuals at boundaries, the constant parameters in Eq. (38) can be reached [7].

2.4.2. Applying the boundary conditions

(a) The boundary conditions are applied for the solution of the differential Eq. (39) as follows:

When x = 0: (Equation 40)

$$u(0)=a_0=u_0;u'(0)=a_1=u_1;u''(0)=a_2=u_2$$

And when x= L:

$$\begin{cases} u(L)=a_0+a_1L+a_2L^2+\ldots+a_nL^n=u_{L_0} \\ u'(L)=a_1+2a_2L+3a_3L^2+\ldots+na_nL^{n-1}=u_{L_1} \\ u''(L)=2a_2+6a_3L+12a_4L^2+\ldots+n(n-1)a_nL^{n-2}=u_{L_2} \end{cases}$$

(Equation 41)

2.4.3. Application of the AGM

Taking into account the AGM, initially, we introduce the residuals [7]:

$$F(\eta)=\left(1+\frac{1}{\beta}\right)f''''(\eta)-\left(\frac{A_1}{A_3}\right)R\left[f'(\eta)f''(\eta)-f(\eta)f'''(\eta)\right]-\left(\frac{A_2}{A_3}\right)Mf''(\eta)$$

$$G(\eta)=\Theta''(\eta)+\left(\frac{3N}{3N+4}\right)\left(\frac{A_5}{A_4}P_rR\right)f(\eta)\Theta'(\eta)-\left(\frac{3N}{3N+4}\right)\left(\frac{A_5}{A_4}P_rR\beta_E\right)\left[f(\eta)f'(\eta)\Theta'(\eta)+f^2(\eta)\Theta''(\eta)\right]+\left(\frac{3N}{3N+4}\right)\left(\frac{A_2}{A_4}P_rME_c\right)f'^2(\eta)+\left(\frac{3N}{3N+4}\right)\left(\frac{A_3}{A_4}P_rE_c\right)\left(1+\frac{1}{\beta}\right)\left[4^2f'^2(\eta)+f''^2(\eta)\right]=0$$

(Equation 42)

The solutions of the equations are considered as:

$$f(\eta)=\sum_{i=0}^{9}a_i^i,\Theta(\eta)=\sum_{i=0}^{9}b_i^i$$

(Equation 43)

Where: R: Dimensionless viscous number, B_0: Magnetic field $\left(kg\cdot s^{-2}\cdot A^{-1}\right)$, A_1,A_2,A_3,A_4,A_5: Dimensionless constants, P: Density $\left(kg/m^3\right)$, μ: Dynamic viscosity (Pas), $\bar{\sigma}$: Cauchy stress tensor, P: Nano-solid-particles, nf: Nanofluid, v: Kinematic viscosity $\left(m^2/s\right)$, v: Velocity in y direction (m/s), P: Pressure term (Pa), M: Dimensionless Magnetic parameter, u: Velocity in x direction (m/s), φ : Solid volume fraction, μ_B: Dynamic plastic viscosity (Pa s), σ_{nf}: Electrical conductivity (siemens /m), x,y: Cartesian coordinates (m), σ: Normal stress, $\bar{\tau}$: Deviatoric stress tensor, N_u^*: Nusselt number, e_{ij}: Deformation rate, f: Base fluid, f', f: Dimensionless velocity.

3. Results and discussion

Table 1. The results obtained using the HPM and the AGM for $-f''(1)$ and $-\theta'(1)$ when $N=1$, $Ec=0.01$, $M=1$, $R=1$, $\delta=0.1$, $\beta=0.8$, $\beta_E=0.5$, $\varphi=0.02$ and $P_r=6.2$.

R	The results obtained using the HPM and the AGM			
	HPM		AGM	
	$-f''(0)$	$-\theta'(0)$	$-f''(0)$	$-\theta'(0)$
0.1	4.06360928	0.83216004	4.06360927	0.83216004
0.2	4.06777559	0.84380209	4.06777565	0.84380167
0.5	4.08027014	0.87944411	4.08027081	0.87943730
0.8	4.09275806	0.91616823	4.09275988	0.91613703
1.0	4.10107958	0.94125739	4.10108251	0.94119108
1.2	4.10939806	0.96683536	4.10940237	0.96671072
1.5	4.12187000	1.00612573	4.12187694	1.00585024

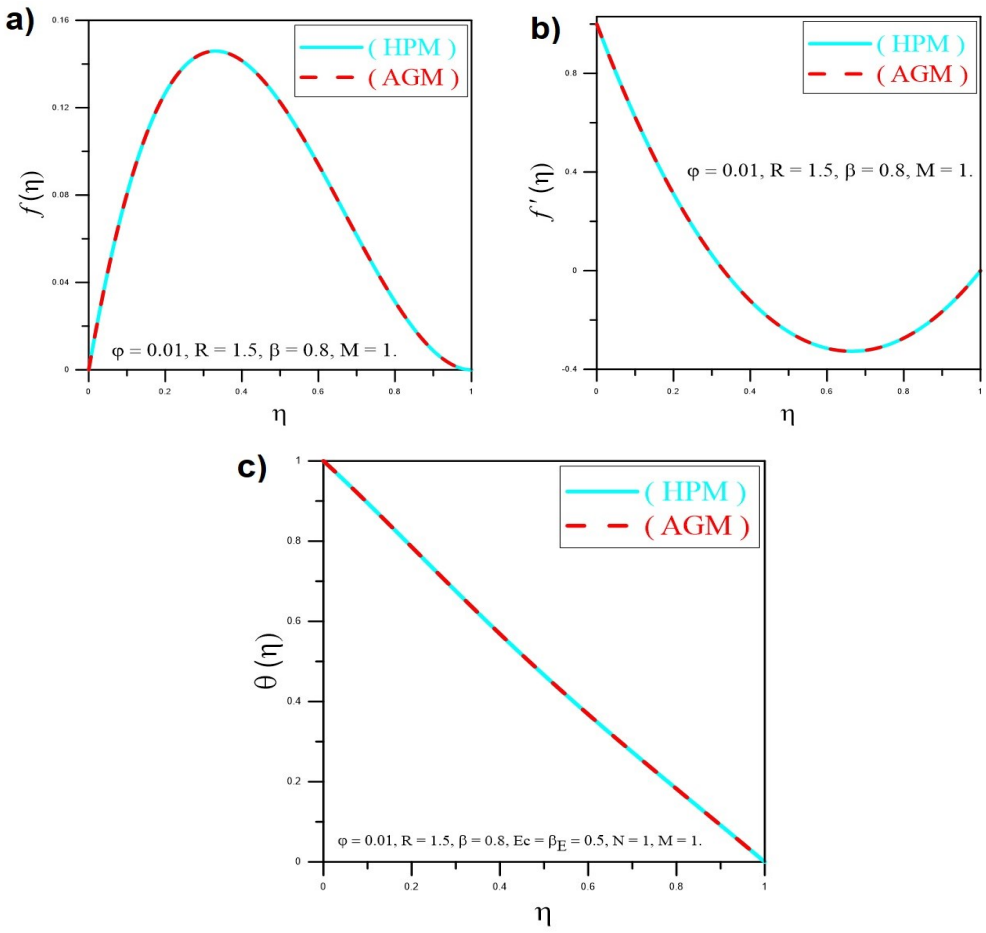

Fig 2. The results acquired using the HPM and the AGM for $f(\eta)$ (a), $f'(\eta)$ (b), and $\theta(\eta)$ (c)

Table 2. Thermophysical characteristics of pure water and various metallic and nonmetallic NPs [7]

	ρ (Kg / m^3)	Cp (J / Kg)	K (W / mK)	σ (S m^{-1})
Cu	8933	385	401	5.96 * 10^7
H_2O	997.1	4179	0.613	0.05
$Al_2 O_3$	3970	765.0	40.000	1* 10^{-10}
Ag	10.500	235	429	6.3 * 10^7
Au	19.300	129	318	4.52 * 10^7

In this study, the impacts of various factors on the heat transfer characteristics and the values of N_u^* calculated for various parameters and metallic and nonmetallic NPs are illustrated in the form of graphs and tables for clarity. To validate the semi-analytical solution obtained using the AGM, the results are compared with those obtained using the HPM. This comparison is depicted in Fig 2 and Table 1. As clearly noticed from Table 1 and Fig 2, the comparison indicates a perfect agreement. Table 2 shows the thermophysical characteristics of pure water and various metallic and nonmetallic NPs.

The change in the TP as a function of casson fluid parameter β is depicted in Fig 3. Fig 3 indicates that the TP decreases with increasing β. The variation in the TP versus the M is graphically presented in Fig 4. It is clear from Fig 4 that the TP increases as the M increases, which is in good agreement with the previous report [40]. This change in the TP can mainly be attributed to the presence of the Joule heating effect, which

leads to the thickening of the temperature boundary layer. Accordingly, it is concluded that higher values of M parameter are more appropriate where the heating is required.

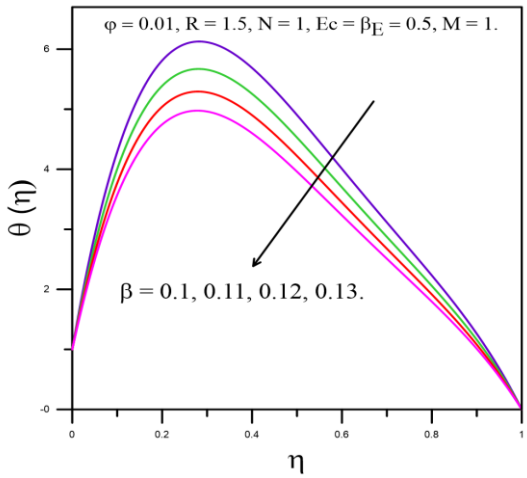

Fig 3. The effect of β on the $\theta(\eta)$

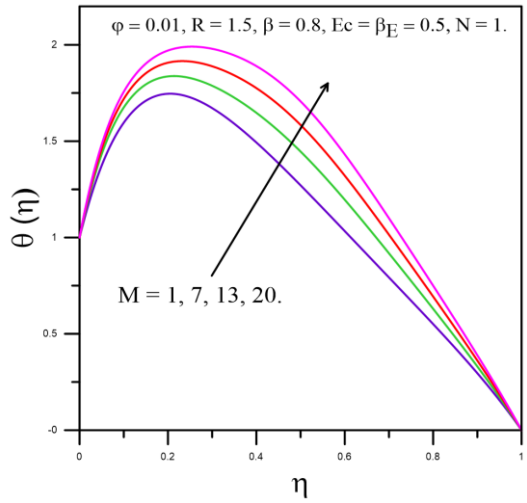

Fig 4. The influence of M on the $\theta(\eta)$

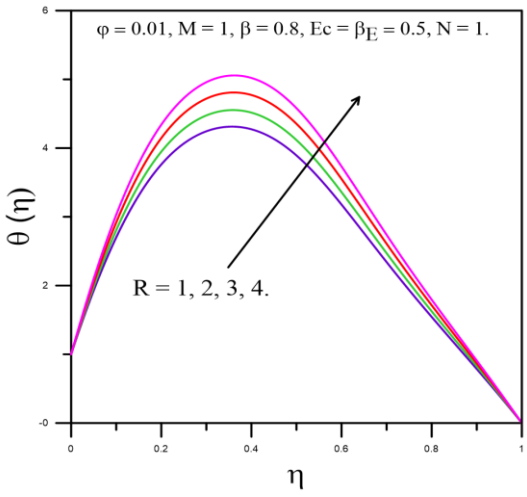

Fig 5. The influence of R on the $\theta(\eta)$

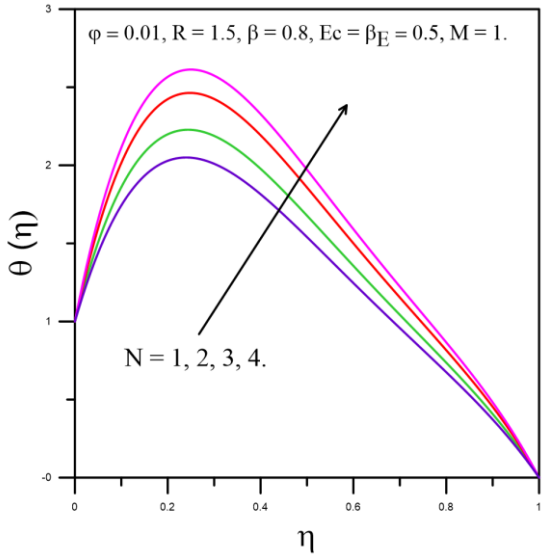

Fig 6. The effect of N on the $\theta(\eta)$

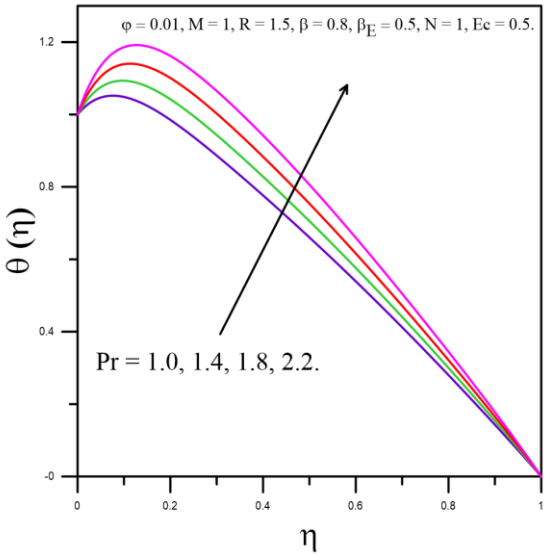

Fig 7. The impact of Pr on the $\theta(\eta)$

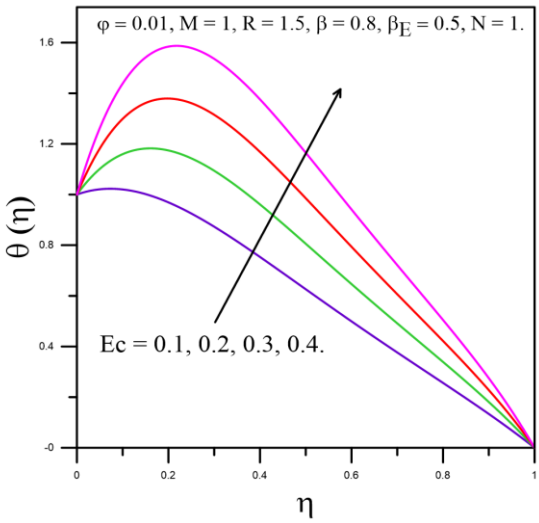

Fig 8. The influence of Ec on the $\theta(\eta)$

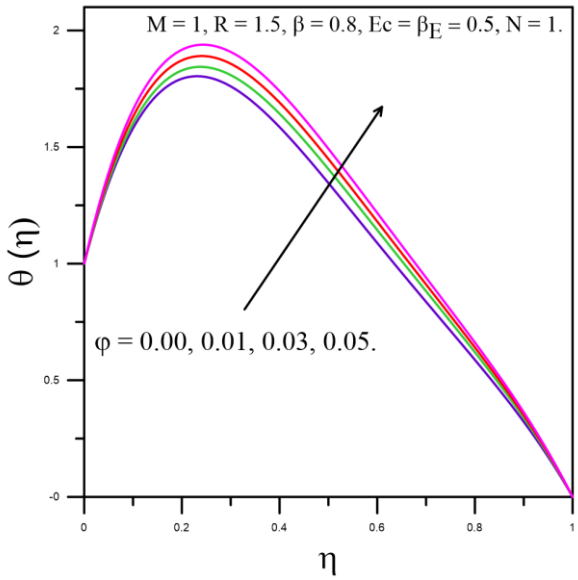

Fig 9. The impact of φ on the $\theta(\eta)$

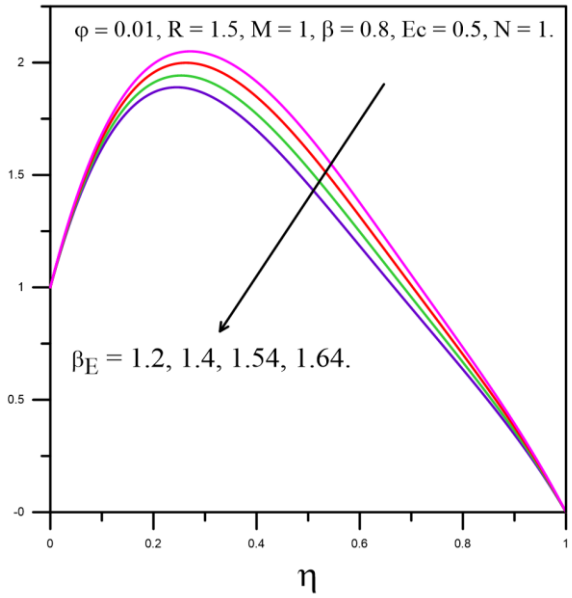

Fig 10. The influence of β_E on the $\theta(\eta)$

Fig 5 illustrates the effect of R on the TP. It is found that there is an increase in the TP with the rise of R.

The effect of N on the TP is presented in Fig 6. Increasing N parameter gives rise to an increment in the TP as observed in Fig 6 which is consistent with the result of a previously published study [40].

Fig 7 depicts the influence of Pr on the TP. As clearly noticed from Fig 7 that the TP increases for large numbers of Pr. The main reason for this change is that a large number of Pr cause a significant reduction in thermal diffusivity and thickness of the thermal boundary layer.

The effect of Ec on the TP is exposed in Fig 8. It is found that the TP increases for increasing values of the Ec. This increase in the TP is expected as the Ec plays a direct role on the heat dissipation process.

Fig 9 indicates the effect of volume fraction parameter φ on the TP. It is clear from Fig 9 that the TP increases with increasing φ. An enhancement in the φ value gives rise to an increment in the friction between nanofluid particles, resulting in an increment in the temperature. These results are found to be identical with those reported in [41].

Fig 10 shows how the β_E affects the TP. The change in the TP is primarily caused by the fact that, as β_E values rise, NPs need more time to transfer heat energy to their neighboring NPs. This explains the non-conductive behavior of the environment and results in the decay of the TP in the flow region. However, when $\beta_E = 0$, the temperature field predominates because $\beta_E = 0$ represents the flow of heat moving at infinite speed. Contrary to the classical Fourier's theory, the TP appears to be suppressed when the CCHF model is used, which is consistent with the report of a published study [30].

Besides, from an industrial point of view, momentum and heat transport coefficients have numerous advantages. The numerical values of N_u^* for different control parameters and various metallic and nonmetallic NPs are calculated when $N = 1$, $E_c = 0.01$, $\varphi = 0.02$, $M = 1$, $\delta = 0.1$, $\beta = 0.8$, $\beta_E = 0.5$ and $P_r = 6.2$. The effect of the R on the N_u^* is presented in Table 3. It is clear from Table 3 that the Nu varies proportionally with the R, which is consistent with the results of a previous study [14].

The variation of N_u^* as a function of the M is shown in Table 4. Table 4 reveals that the N_u^* is

inversely proportional to the M. This result is in good agreement with that reported in [14].

Table 3. The influence of the R on the N_u^*.

R	N_u^*
0.1	0.37837326
0.2	0.38366676
0.5	0.39987276
0.8	0.41657078
1.0	0.42797852
1.2	0.43960852
1.5	0.45747339

Table 4. The variation of N_u^* as a function of the M

M	N_u^*
0.1	0.42883319
0.2	0.42873799
0.5	0.42845276
0.8	0.42816805
1.0	0.42797852
1.2	0.42778922
1.5	0.42750570

Table 5. The N_u^* values with respect to the φ

φ	N_u^*
0.00	0.41219198
0.01	0.42287993
0.02	0.43376565
0.03	0.44485357
0.04	0.45614831
0.05	0.46765462

Table 6. The values of N_u^* for various metallic and nonmetallic NPs

NPs	N_u^*
Au	0.43276765
Cu	0.42797852
Ag	0.42711319
Al_2O_3	0.42693013

The N_u^* values against the φ values are given in Table 5. The results show that the N_u^* changes proportionally with the φ. Similar enhancement in the N_u^* with increasing φ was also reported for Al_2O_3-water nanofluid in a triangular duct and Al_2O_3-water and TiO_2-water nanofluids in turbulent flow in previous experimental and numerical studies [42,43].

The N_u^* values for various metallic (Ag, Cu, and Au) and nonmetallic (Al_2O_3)NPs are also determined and the obtained results are shown in Table 6. As distinctly noticed from Table 6, different metallic and nonmetallic NPs have different values of the N_u^*.

4. Conclusion

This work highlights the effect of various factors such as β, R, M, φ, N, Pr, E_c, and β_E on the heat transfer characteristics of the steady MHD Casson nanofluid (Cu + Water) between two infinite parallel plates considering the CCHF model. The governing equations are solved by means of the AGM. The values of the N_u^* are also determined for the R, M, and φ parameters and various metallic and nonmetallic NPs. There is a perfect agreement between the results obtained using the AGM and the HPM, confirming the accuracy of the AGM. The important findings obtained within the scope of this study are as follows:

- Rising M causes an increment in the TP, indicating that higher values of M are more appropriate where the heating is required.

-The TP decreases with increasing β while it increases with increasing R.

- Increasing N, Pr, Ec, and φ result in an increment in the TP.

- A decreasing trend in the TP is found for large values of the β_E.

- The N_u^* varies proportionally with the R and φ parameters, but it is inversely proportional to the M parameter.

- Different metallic and nonmetallic NPs have different values of the N_u^* .

Author Contributions:

A. El Harfouf: Conceptualization, Methodology, Investigation, Validation, Writing-original draft-review & editing, Formal analysis.

Dung Nguyen Trong: Writing-original draft-review & editing-review.

Hassane Mes-adi: Writing-original draft.

S. Hayani Mounir: Writing-original draft.

Umut Saraç: Writing-original draft-review & editing-editing.

Doan Phuong Lan: Writing-original draft.

Van Cao Long: Writing-original draft.

Ştefan Ţălu: Writing-original draft & editing-review.

All authors have read and agreed to the published version of the manuscript.

Funding: This research received no external unding.

Data Availability Statement: The data that support the findings of this study are available from the corresponding author upon reasonable request.

Conflicts of Interest: The authors declare no conflict of interest.

ORCID:

A. El Harfouf, https://orcid.org/0002-9836-4923

Dung Nguyen Trong, http://orcid.org/0000-0002-7706-1392

Hassane Mes-adi, https://orcid.org/0000-0003-4315-9786

S. Hayani Mounir, http://orcid.org/0000-0001-6014-9702

Umut Saraç, https://orcid.org/0000-0001-7657-173X

Doan Phuong Lan, https://orcid.org/0000-0002-6514-3657

Van Cao Long, https://orcid.org/0000-0002-0885-302X

Ştefan Ţălu, http://orcid.org/0000-0003-1311-7657

References

[1] M. Azam. (2022). Effects of Cattaneo-Christov heat flux and nonlinear thermal radiation on MHD Maxwell nanofluid with Arrhenius activation energy. *Case Studies in Thermal Engineering*, 34, 102048.

[2] A. Alhadhrami, C.S. Vishalakshi, B.M. Prasanna et al. (2021). Numerical simulation of local thermal non-equilibrium effects on the flow and heat transfer of non-Newtonian Casson fluid in a porous media. *Case Studies in Thermal Engineering*, 28, 101483.

[3] U.S. Mahabaleshwar, T. Maranna and F. Sofos. (2022). Analytical investigation of an incompressible viscous laminar Casson fluid flow past a stretching/shrinking sheet. *Scientific Reports*, 12, 18404.

[4] G.M. Moatimid, M.A.A. Mohamed and K. Elagamy. (2022). A Casson nanofluid flow within the conical gap between rotating surfaces of a cone and a horizontal disc. *Scientific Reports*, 12, 11275.

[5] A.C.V. Ramudu, K.A. Kumar, V. Sugunamma et al. (2020). Heat and mass transfer in MHD Casson nanofluid flow past a stretching sheet with thermophoresis and Brownian motion. *Heat Transfer*, 49(8), 5020-5037.

[6] I.A. Shah, S. Bilal, M.I. Asjad et al. (2022). Convective Heat and Mass Transport in Casson Fluid Flow in Curved Corrugated Cavity with Inclined Magnetic Field. *Micromachines*, 13(10), 1624.

[7] A. El Harfouf, S.H. Mounir and A. Wakif. (2023). Steady Magnetohydrodynamic Casson Nanofluid Flow Between Two Infinit Parallel Plates Using Akbari Ganji's Method (AGM). *Journal of Nanofluids*, 12(3), 633-642.

[8] M.D. Shamshuddin, S.R. Mishra and T Thumma. (2019). Chemically Reacting Radiative Casson Fluid Over an Inclined Porous Plate: A Numerical Study. *Numerical Heat Transfer and Fluid Flow*, 469-479.

[9] R. Vijayaragavan and M.A. Kavitha. (2018). Heat and Mass Transfer in Unsteady MHD Casson Fluid Flow past an Inclined Plate with

Thermal Radiation and Heat source/sink. *Research Journal of Engineering and Technology*, 9(2), 214-223.

[10] A. Zeeshan, M. Awais and F. Alzahrani. (2021). Energy analysis of non-Newtonian nanofluid flow over parabola of revolution on the horizontal surface with catalytic chemical reaction. *Heat Transfer*, 50(6), 6189-6209.

[11] A.S. Dogonchi, M. Waqas, S.R. Afshar et al Int. (2020). Investigation of magneto-hydrodynamic fluid squeezed between two parallel disks by considering Joule heating, thermal radiation, and adding different nanoparticles. *International Journal of Numerical Methods for Heat & Fluid Flow*, 30(2), 659-680.

[12] T. Tayebi, A.S. Dogonchi and N Karimi et al. (2021). Thermo-economic and entropy generation analyses of magnetic natural convective flow in a nanofluid-filled annular enclosure fitted with fins. *Sustainable Energy Technologies and Assessments*, 46, 101274.

[13] A.J. Chamkha, A.S. Dogonchi and D.D. Ganji. (2018). Magnetohydrodynamic Nanofluid Natural Convection in a Cavity under Thermal Radiation and Shape Factor of Nanoparticles Impacts: A Numerical Study Using CVFEM. *Applied Sciences*, 8(12), 2396.

[14] M. Sheikholeslami, M.M. Rashidi, D.M. Al Saad et al. (2016). Steady nanofluid flow between parallel plates considering thermophoresis and Brownian effects. *Journal of King Saud University – Science*, 28(4), 380-389.

[15] S. Sivasankaran, T. Chandrapushpam, M. Bhuvaneswari et al. (2022). Effect of chemical reaction on double diffusive MHD squeezing copper water nanofluid flow between parallel plates. *Journal of Molecular Liquids*, 368(B), 120768.

[16] H.A.H. Asfour and M.G. Ibrahim. (2023). Numerical simulations and shear stress behavioral for electro-osmotic blood flow of magneto Sutterby nanofluid with modified Darcy's law. *Thermal Science and Engineering Progress*, 37, 101599.

[17] M.G. Ibrahim and M.Y. Abou-zeid. (2022). Influence of variable velocity slip condition and activation energy on MHD peristaltic flow of Prandtl nanofluid through a non-uniform channel. *Scientific Reports*, 12, 18747.

[18] A. El Harfouf, A. Wakif and S.H. Mounir. (2020). Analytical and Numerical Analysis of Magneto Hydrodynamic Flow and Heat Transfer in a Nanofluid via the Christov-Cattaneo Heat Flux Theory. *Sensor Letters*, 18(8), 643-657.

[19] A. El Harfouf, A. Wakif and S.H. Mounir. (2020). Heat Transfer Analysis on Squeezing Unsteady MHD Nanofluid Flow Between Two Parallel Plates Considering Thermal Radiation, Magnetic and Viscous Dissipations Effects a Solution by Using Homotopy Perturbation Method. *Sensor Letters*, 18(2), 113-121.

[20] A. El Harfouf, A. Wakif and S.H. Mounir. (2021). Semi-Analytical Resolution of a Squeezing Unsteady Nanofluid Flow Between Two Parallel Plates Using Homotopy Perturbation Method (HPM). *Wseas Transactions on Heat and Mass Transfer*, 16, 1-13.

[21] Z. Shah, S. Islam, T. Gul et al. (2018). The electrical MHD and Hall current impact on micropolar nanofluid flow between rotating parallel plates. *Results in Physics*, 9, 1201-1214.

[22] A. Jafarimoghaddam. (2019). On the Homotopy Analysis Method (HAM) and Homotopy Perturbation Method (HPM) for a nonlinearly stretching sheet flow of Eyring-Powell fluids. *Engineering Science and Technology, an International Journal*, 22(2), 439-451.

[23] H. Mirgolbabaee, S.T. Ledari and D.D. Ganji. (2016). New approach method for solving Duffing-type nonlinear oscillator. *Alexandria Engineering Journal*, 55(2), 1695-1702.

[24] W.A. Khan, A.M. Rashad, S.M.M. EL-Kabeir,

A.M.A. EL-Hakiem. (2020). Framing the MHD Micropolar-Nanofluid Flow in Natural Convection Heat Transfer over a Radiative Truncated Cone. *Processes*, 8(4), 379.

[25] A.S. Dogonchi and D.D. Ganji. (2018). Effect of Cattaneo–Christov heat flux on buoyancy MHD nanofluid flow and heat transfer over a stretching sheet in the presence of Joule heating and thermal radiation impacts. *Indian Journal of Physics*, 92, 757-766.

[26] S. Han, L. Zheng, C. Li, X. Zhang. (2014). Coupled flow and heat transfer in viscoelastic fluid with Cattaneo–Christov heat flux model. *Applied Mathematics Letters*, 38, 87-93.

[27] Z. Li. (2012). A new constant heat flux model for vertical U-tube ground heat exchangers. *Energy and Buildings*, 45, 311-316.

[28] M. Khan and W.A. Khan. (2016). Three-dimensional flow and heat transfer to burgers fluid using Cattaneo-Christov heat flux model. *Journal of Molecular Liquids*, 221, 651-657.

[29] S.R.R. Reddy, P.B.A. Reddy and A.M. Rashad. (2021). Effectiveness of binary chemical reaction on magneto-fluid flow with Cattaneo–Christov heat flux model. *Proceedings of the Institution of Mechanical Engineers, Part C: Journal of Mechanical Engineering Science*, 235(12), 2192.

[30] A.S. Dogonchi and D.D. Ganji. (2017). Impact of Cattaneo–Christov heat flux on MHD nanofluid flow and heat transfer between parallel plates considering thermal radiation effect. *Journal of the Taiwan Institute of Chemical Engineers*, 80, 52-63.

[31] M. Sheikholeslami and D.D. Ganji. (2017). Impact of electric field on nanofluid forced convection heat transfer with considering variable properties. *Journal of Molecular Liquids*, 229, 566-573.

[32] M. Sheikholeslami. (2017). Numerical simulation of magnetic nanofluid natural convection in porous media. *Physics Letters A*, 381(5), 494-503.

[33] M. Sheikholeslami. (2018). Magnetic source impact on nanofluid heat transfer using CVFEM. *Neural Computing and Applications*, 30, 1055-1064.

[34] D.N. Trong, C.N. Chinh and H.T. Vinh. (2017). Molecular dynamics study of microscopic structures, phase transitions and dynamic crystallization in Ni nanoparticles. *RSC Advances*, 7, 25406-25413.

[35] T.T. Quoc, D.N. Trong, V.C. Long, U. Sarac and S. Talu. (2022). A Study on the Structural Features of Amorphous Nanoparticles of Ni by Molecular Dynamics Simulation. *Journal of Composites Science*, 6(9), 278.

[36] D.N. Trong and V.C. Long. (2021). Effects of Number of Atoms, Shell Thickness, and Temperature on the Structure of Fe Nanoparticles Amorphous by Molecular Dynamics Method. *Advances in Civil Engineering*, 9976633, 1-12.

[37] D.N. Trong and P.N. Tri. (2020). Factors affecting the structure, phase transition and crystallization process of AlNi nanoparticles. *Journal of Alloys and Compounds*, 812, 152133.

[38] D.N. Trong. (2018). Influence of impurity concentration, atomic number, temperature and tempering time on microstructure and phase transformation of Ni1−xFex (x = 0.1, 0.3, 0.5) nanoparticles. *Modern Physics Letters B*, 32(18), 1850204.

[39] H. Attari and A. Yazdani. (2011). A computational method for fuzzy Volterra-Fredholm integral equations. *Fuzzy Information and Engineering*, 3(2), 147-156.

[40] A.S. Dogonchi, K. Divsalar and D.D. Ganji. (2016). Flow and heat transfer of MHD nanofluid between parallel plates in the presence of thermal radiation. *Computer Methods in Applied Mechanics and Engineering*, 310, 58-76.

[41] K. Das. (2014). Flow and heat transfer characteristics of nanofluids in a rotating frame. *Alexandria Engineering Journal*, 53(3), 757-766.

[42] B.C. Pak and Y.I. Cho. (1998). Hydrodynamic and heat transfer study of dispesed fluids with submicron metallic oxide particles. *Experimental Heat Transfer*, 11(2), 151-170.

[43] S.Z. Heris, S.H. (2011). Noie, E. Talaii, J. Sargolzaei. Numerical investigation of Al_2O_3/water nanofluid laminar convective heat transfer through triangular ducts. *Nanoscale Research Letters*, 6, 179.